Hybrid Systems for N-body Simulations

Spinnato, P.F.

Publication date
2003

Chapter 5

The Efficiency of the Spiral-in of a Black Hole to the Galactic Centre[†]

In this chapter, we use the direct particle-particle method, the treecode, and the particle-mesh code, introduced in section 1.2 and 1.4, to study the efficiency at which a black hole or dense star cluster spirals in to the Galactic centre. As introduced in section 1.7, this process is driven by a drag force, called dynamical friction, that results from the combined gravitational pull exerted by a star distribution on a massive body moving through the system.

This phenomenon takes place on a dynamical friction time scale, which depends on the value of the so-called Coulomb logarithm ($\ln \Lambda$). We determine the accurate value of this parameter using the three methods mentioned above with up to two million plus one particles. We find that the three different techniques are in excellent agreement. Our result for the Coulomb logarithm appears to be independent of the number of particles. We conclude that $\ln \Lambda = 6.6 \pm 0.6$ for a massive point particle in the inner few parsec of the Galactic bulge. For an extended object, like a dense star cluster, $\ln \Lambda$ is smaller, with a value of the logarithm argument Λ inversely proportional to the object size.

5.1 Introduction

The region near the Galactic centre is populated by very young objects, such as the Quintuplet star cluster (Nagata *et al.*, 1990; Okuda *et al.*, 1990), the Arches cluster (Nagata *et al.*, 1995) and the central star cluster (Tamblyn & Rieke, 1993; Krabbe *et al.*, 1995), which are of considerable interest for the astronomical community. One of the more interesting conundrums is the presence of stars as young as few Myr (Tamblyn & Rieke, 1993;

[†]This chapter is based on work published in:
P.F. Spinnato; M. Fellhauer and S.F. Portegies Zwart: *The Efficiency of the Spiral-in of a Black Hole to the Galactic Centre*, Monthly Notices of the Royal Astronomical Society, in press, 2003.

Krabbe *et al.*, 1995) within a parsec from the Galactic centre (Gerhard, 2001). *In situ* formation is problematic, due to the strong tidal field of the Galaxy, which makes this region inhospitable for star formation. One possible solution is provided by Gerhard (2001), who proposes that a star cluster of 10^6 $M_\odot$, where $M_\odot$ is a solar mass, spirals in to the Galactic centre within a few million years from a distance $\gtrsim 30$ pc. The infall process is driven by dynamical friction (Chandrasekhar, 1943). A quantitative analysis of this model by McMillan & Portegies Zwart (2003) confirms Gerhard's results. The main uncertainty in the efficiency of dynamical friction, and therewith the time scale for spiral-in, is hidden in a single parameter, called the Coulomb logarithm $\ln\Lambda$. Accurate determination of this parameter is crucial for understanding this process. Nevertheless, a precise value of $\ln\Lambda$ for the Galactic central region is not available. In the work presented in this chapter, we determine $\ln\Lambda$ for the Galactic centre. We focus on the efficiency of the interaction between an intermediate mass black hole (BH hereafter) and the stars in the Galactic central region. In section 5.4 we comment on how this approach can be applied to star clusters that sink to the Galactic centre.

Dynamical friction is important for a large variety of astronomical phenomena, e.g. planet migration (Goldreich & Tremaine 1980; Cionco & Brunini 2002), core collapse in dense star clusters (Portegies Zwart *et al.*, 1999) or mergers in galaxy clusters (Makino 1997; Cora *et al.* 1997; van den Bosch *et al.* 1999). The physics of the infall process of a satellite in the parent galaxy is basically the same as in the case of a BH spiralling in to the Galactic centre. The relevant parameters, however, are quite different in the two cases. For example, an inspiraling galaxy has finite size, whereas a BH is a point mass. Dynamical friction also plays an important role in the evolution of the black hole binary formed after the merging of two galaxies both hosting a BH at their centre (Milosavljević & Merritt, 2001). In this case, dynamical friction is important in the early phase of galaxy merging, when the BHs orbits converge and become bound.

In the classical study of Chandrasekhar (1943), dynamical friction is driven by the drag force experienced by a point mass moving through an infinite medium of homogeneous density. The consequences of finiteness and non-homogeneity have been analysed in various works (see Maoz 1993; Milosavljević & Merritt 2001). Just & Peñarrubia (2003) carried out an analytical study of dynamical friction in inhomogeneous systems, leading to a value of the Coulomb logarithm that depends on the infalling object position. Colpi & Pallavicini (1998) developed a general theoretical framework for the interaction of a satellite with a primary galaxy, able to describe dynamical friction in finite, inhomogeneous systems. They applied their theory of linear response to orbital decay of satellites onto a spherical galaxy (Colpi, 1998) and short-lived encounters with a high-speed secondary (Colpi & Pallavicini, 1998). They studied evolution of satellites in isothermal spherical haloes with cores (Colpi *et al.*, 1999), extended in Taffoni *et al.* (2003), treating satellite finite size and mass loss. Still, the original expression of Chandrasekhar is used to model dynamical friction in many astronomical situations (see Binney & Tremaine 1987, § 7.1; Hashimoto *et al.* 2003). The cases we study here are characterised by a point mass, with a very small mass compared to the primary system. Therefore Chandrasekhar's formulation is appropriate in our cases.

We determine the value of $\ln\Lambda$ for a BH spiralling-in to the Galactic centre by means

of self-consistent N-body simulations. This is by far not an easy task. N-body models either lack in the number of particles (a direct N-body code can treat up to about 10^5 particles, compared to 10^8 for the real system) or have to introduce softening (Aarseth, 1963) and approximation of the force calculation (treecode (Barnes & Hut, 1986) or particle-mesh code (Hockney & Eastwood, 1988)). The softening parameter ϵ was introduced to limit the strength of the mutual gravitational interaction during close stellar encounters. Without softening, the very high accelerations experienced by the encountering bodies would cause very tiny integration steps, which would result in a n effective freeze of the global system evolution, with consequent dramatic performance degradation. The use of this approximation should not invalidate the numerical results, as long as the simulated system is studied on a time scale shorter than the relaxation time scale (Binney & Tremaine 1987, ch. 4, see also discussion in section 5.3.4 below). The dynamical friction time scale of the systems we simulate is in all cases shorter than the relaxation time scale, so we can safely use the approximate methods.

Nevertheless, since close encounters have an important effect on dynamical friction, decreasing their strength by means of softening also decreases the strength of dynamical friction, i.e. lowers the value of $\ln \Lambda$. The same role of softening is played, in the particle-mesh code, by the grid cell size l.

Our methodological approach for the present work (see fig. 5.1) consists of comparing the "exact" results obtained with the direct method for low particle numbers (up to 80 000) with the results of the treecode, which are less accurate and are influenced by force softening, to understand how the softening ϵ influences the results and how they have to be scaled according to the value of ϵ. Then the results of the treecode are compared to the results of the particle-mesh code, to see how softening (tree) and grid-resolution l (particle-mesh) can be compared and scaled. Finally, having the right scaling between the different codes, we will be able to perform high particle number simulations (up to $4 \cdot 10^7$) with the particle-mesh code to obtain the value of the Coulomb logarithm for the inner Galactic Bulge.

5.2 Methods and model

5.2.1 Direct method

For our direct N-body calculations we used the `kira` integrator module of the Starlab software environment[1] (Portegies Zwart *et al.*, 2001), introduced in section 1.4. Conceived and written as an independent alternative to Aarseth's NBODY4 and NBODY5 (Aarseth, 1985, 1999), the workhorses of collisional N-body calculations for the past 25 years, `kira` is a high-order predictor-corrector scheme designed for simulations of collisional stellar systems. This integrator incorporates a Hermite integration scheme (Makino & Aarseth, 1992) and a block time step scheduler (McMillan, 1986) that allows homogeneous treatment of all objects in the system.

While `kira` is designed to operate efficiently on general-purpose computers, it achieves

[1] See: `http://manybody.org`

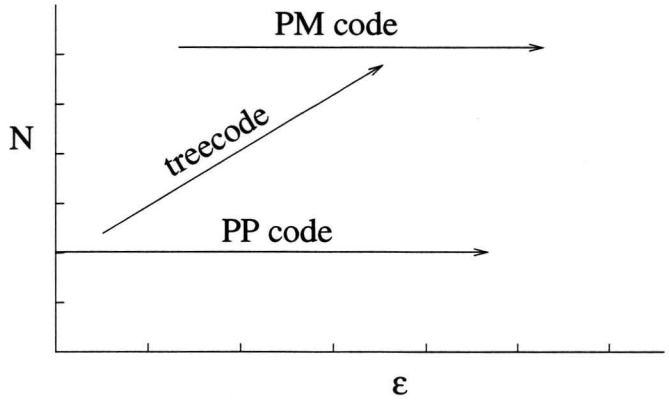

Figure 5.1: A sketch of the strategy that we adopt in order to explore the ϵ-N parameter space.

by far its greatest speed when combined with GRAPE-6 special purpose hardware[2] (see section 1.3). For the work presented here we performed simulations with the GRAPE-6 system at the University of Tokyo with up to 80 000 particles.

5.2.2 Treecode

The hierarchical treecode is widely used for the simulation of collisionless systems. We described it in section 1.4.2, and studied it extensively in chapter 3 and 4. Our treecode simulations were initially performed with both a code written by Jun Makino (Makino, 1991b), and with GADGET (Springel *et al.*, 2001). We also used GADGET in the performance simulation work described in section 3.4.3, and in the pseudo-particle treecode accuracy analysis in section 4.3.4. In GADGET each particle is assigned an individual time-step, and at each iteration only those particles having an update time below a certain time are selected for force evaluation. This criterion was originally introduced in the direct N-body code (see section 2.3.1).

This code is parallelized using MPI (Message Passing Interface Forum, 1997). In the parallel version, the geometrical domain is partitioned, and each processor hosts the particles located in the domain partition assigned to it. The computation of forces on the selected i-particles is performed by scattering the particle data to remote processors. Then partial forces from the particles hosted by the remote processors are computed locally. Finally, calculated forces are received back by the i-particle host, and added up resulting in the total force on the i-particles. We run our parallel treecode simulations on the DAS-2 distributed supercomputer, mentioned in section 2.2.1.

[2]See: `http://www.astrogrape.org`

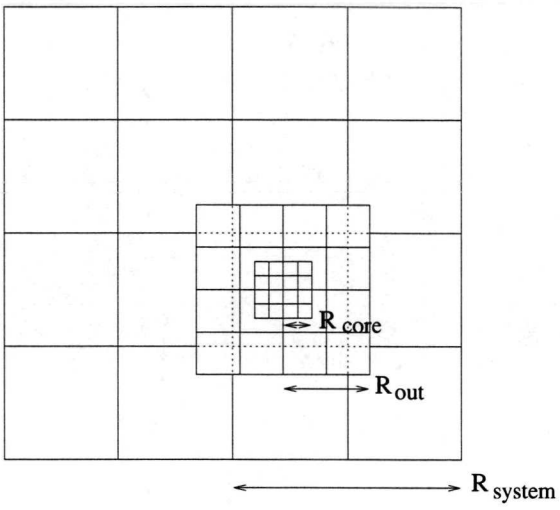

Figure 5.2: The different grids of SUPERBOX for a number of cells per dimension $n = 4$. The finest and intermediate grids are focussed on the object of interest. Each grid is surrounded by a layer of two halo cells. Such haloes are not shown here.

5.2.3 Particle-mesh code

To perform calculations using several millions of particles we use a particle-mesh (PM) code named SUPERBOX (Fellhauer *et al.*, 2000). As mentioned in section 1.2, in the particle-mesh technique densities are derived on Cartesian grids. Using a fast Fourier transform algorithm these densities are converted into a grid-based potential. Forces acting on the particles are calculated using these grid-based potentials, making the code nearly collisionless. SUPERBOX in particular completely neglects two-body relaxation, causing it to retain only a small amount of grid-based relaxation (Fellhauer *et al.*, 2000).

The adopted implementation incorporates some differences to standard PM-codes. State-of-the-art PM codes use a cloud-in-cell (CIC) scheme to assign the masses of the particles to the grid cells. Therefore the mass of a particle i is split up into neighbouring cells according to its distance to the centre of the cell. Forces are then calculated by adding up the same fractions of the forces from all cells to particle i. In contrast, SUPERBOX uses the "old-fashioned" nearest-grid-point scheme, where the total mass of the particle is assigned to the grid cell the particle is located in. Forces acting on the particle are then calculated only from the forces acting on this particular cell. To achieve similar precision as CIC, SUPERBOX uses space derivatives up to the second order to compute the forces.

To achieve high resolution at the places of interest, SUPERBOX incorporates for every simulated object (e.g. each galaxy and/or star cluster or disc, bulge and halo) two levels of sub-grids co-moving with the objects of interest while the latter are moving through the

simulated area (see fig. 5.2). This provides higher resolution only where it is necessary.

5.2.4 The theory of the Coulomb logarithm

Dynamical friction affects a mass moving in a background sea of lower mass objects. A practical expression for the strength of the drag force on a point particle with mass M_{BH} is (Binney & Tremaine 1987, p. 424):

$$\frac{d\mathbf{v}_{BH}}{dt} = -4\pi G^2 \ln\Lambda \rho M_{BH} \frac{\mathbf{v}_{BH}}{v_{BH}^3} \left[\mathrm{erf}(X) - \frac{2X}{\sqrt{\pi}} e^{-X^2}\right]. \tag{5.1}$$

Here $X = v_{BH}/(\sqrt{2}\sigma)$, where σ is the Maxwellian velocity dispersion, and ρ the background stellar density.

The classical value of Λ is (Binney & Tremaine 1987, p. 423)

$$\Lambda = \frac{b_{max} v_{typ}^2}{G(M_{BH} + m)} \quad . \tag{5.2}$$

Here b_{max} is the largest possible impact parameter for an encounter between the massive point particle and a member of the background population, v_{typ} is the typical speed of the objects in the background population, and m is the mass of each of the background stars. Eq. (5.2) can then be generalised to

$$\Lambda = \frac{b_{max}}{b_{min}} \quad . \tag{5.3}$$

Here b_{min} is the distance below which an encountering particle is captured, instead of being scattered by the massive object. It is somewhat smaller than the 90° turn-around distance. With the direct N-body technique, Λ can be measured precisely. However, with approximate N-body methods, such as the treecode or the PM code, we have to take care of the interference of the softening length/cell size with b_{min}, as discussed in section 5.2.5.

McMillan & Portegies Zwart (2003) obtained an analytic expression for the distance $r(t)$ of the BH to the Galactic centre, with the assumptions that the BH's orbits are nearly circular, and the mass profile of the Galaxy is given by a power law:

$$M(R) = AR^{\alpha} \, . \tag{5.4}$$

They obtained:

$$r(t) = R_0 \left[1 - \frac{\alpha(\alpha+3)}{\alpha+1} \sqrt{\frac{G}{AR_0^{\alpha+3}}} \, \chi \, M_{BH} \, \ln\Lambda \, t\right]^{\frac{2}{3+\alpha}} \quad , \tag{5.5}$$

where

$$\chi = \mathrm{erf}(X) - \frac{2X}{\sqrt{\pi}} e^{-X^2} \quad \text{and} \quad X = \frac{v_{BH}}{\sqrt{2}\,\sigma} \, ,$$

σ being the velocity dispersion. In McMillan & Portegies Zwart (2003) the value of X in the Galactic centre is also computed, resulting in $X = \sqrt{2-\alpha}$. Finally, we take R_0 equal to the half-mass radius of our system R_{hm} (see section 5.2.6). The best fit of eq. (5.5) on the simulation data gives the value of $\ln\Lambda$ for that simulation. The values obtained, for all simulation performed, are reported in the last column of tables 5.3, 5.4 and 5.5.

5.2.5 The role of softening in the determination of the Coulomb logarithm

Softening was introduced in numerical stellar dynamics to limit the strength of mutual forces during close stellar encounters, mainly for computational performance purposes. It consists in a modification of the Newton law for the gravity exerted by a particle j on a particle i, as follows:

$$\mathbf{a}_i = G\frac{m_j}{(r_{ij}^2+\epsilon^2)^{(3/2)}}\mathbf{r}_{ij}\ , \tag{5.6}$$

where $\mathbf{r}_{ij} = \mathbf{r}_j - \mathbf{r}_i$, and ϵ is the softening parameter. As $\mathbf{r}_{ij} \to 0$, the presence of ϵ causes the force to change from inverse square to elastic, with constant Gm_im_j/ϵ^3. In this way the strength of the mutual force between encountering particles is limited.

Softening was first used by Aarseth (1963) in a particle-particle (PP) context (see fig. 1.1 and caption therein). Accuracy requirements soon led to a more precise treatment of close encounters and binaries by means of an analytic approach (Kustaanheimo & Stiefel 1965; Aarseth 1972; Mikkola & Aarseth 1990). The softened force in eq. (5.6) is used in the treecode, where high accuracy in close encounters treatment is not essential. Here we will use the softening both in the treecode simulations, where it is necessary, and in the PP code simulations, where it is used to compare the results of the two codes, in order to study the relation between ϵ and $\ln\Lambda$.

For the PM code, as described in section 5.2.3, force is not computed by using the Newton force, or the softened force in eq. (5.6). Instead, the fact that the gravitational potential on each grid point of the mesh is obtained from a density field defined on the same mesh, leads to an accuracy for the force on each particle limited by the cell size of the grid, l.

Here, we are concerned with the accuracy of the computation of the encounters experienced by a black hole spiralling-in to the Galactic centre. Since the softening (PP and treecode) and the cell size (PM code) affect this accuracy, we will use ϵ and l to quantify the accuracy decrement in our simulations. In section 5.3.5 we will study quantitatively the dependence of $\ln\Lambda$ on ϵ and l.

The reference value for ϵ in the work presented here will be $\epsilon_0 = 0.003\,735$ (units given below in table 5.1). This value, according to Athanassoula *et al.* (2000), is of the same order of magnitude as the optimal softening for a Dehnen sphere distribution (Dehnen, 1993). This distribution is similar to the power law distribution that we use, at least for what concerns the high central density peak, which is the key physical factor in the determination of the optimal softening. For an 80 000 particle distribution, ϵ_0 is about 15 times smaller than

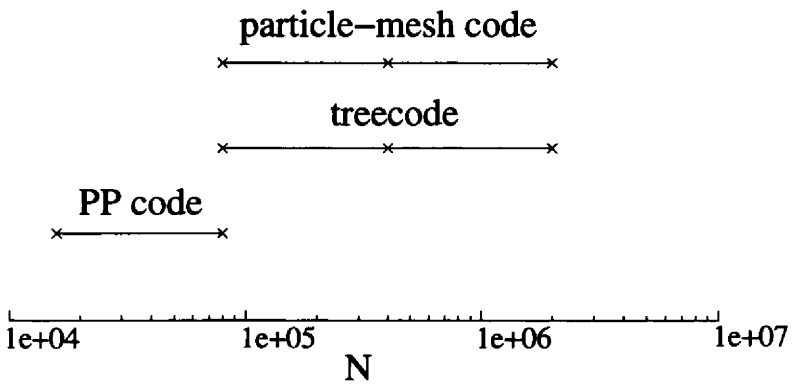

Figure 5.3: Particle ranges for the simulations performed by each method. Crosses denote the particle values used.

the mean inter-particle distance ℓ at the initial BH position $R_0 \simeq 0.87$ (see section 5.2.6). This value for ϵ is small enough to avoid spurious effects in the force between a star and its neighbours, but is sufficient to inhibit very close encounters. The expression for ℓ can be obtained as:

$$\ell = n^{-\frac{1}{3}} = \left(\frac{\rho}{m}\right)^{-\frac{1}{3}} = \sqrt[3]{\frac{4\pi R^{3-\alpha}}{NA\alpha}}\,, \tag{5.7}$$

where n is the star number density, and

$$\rho = \frac{1}{4\pi R^2}\frac{dM}{dR} = \frac{A\alpha}{4\pi}R^{\alpha-3}\,.$$

We used the expression in eq. (5.4) for M, and the fact that the N stars in the system have the same mass $m = 1/N$.

One of the effects of softening is a damping in the BH infall at very small values of the galactocentric distance, more noticeable as N increases. This can be explained with the fact that the inter-particle distance ℓ decreases as the BH approaches the Galactic centre (see eq. 5.7). When ℓ becomes comparable to 2ϵ, the role of softening in the force equation becomes dominant, since particles begin to "overlap". With $N = 400\,000$, we get $\ell = 2\epsilon_0$ when $R \simeq 0.064$, which is close to the value at which the damping arises, as fig. 5.13 below clearly shows.

5.2.6 Initial condition

We generate the initial mass distribution according to the power law given by eq. (5.4), with $\alpha = 1.2$, which reproduces the mass distribution in the centre of the Galaxy, according to Mezger *et al.* (1999). The scale factor is $A = 4.25 \cdot 10^6 \mathrm{M}_\odot$, corresponding to 0.44 in the N-body standard units (Heggie & Mathieu, 1985), which are reported in table 5.1. We use the standard units hereafter, unless other units are explicitly reported. The distributions

$$
\begin{aligned}
G &= 1\ [\mathrm{V}]^2[\mathrm{L}]/[\mathrm{M}] \\
&\equiv 4.3007 \cdot 10^{-3}\ \mathrm{km^2 pc/s^2 M_\odot} \\
&\equiv 4.49842 \cdot 10^{-3}\ \mathrm{pc^3/Myr^2 M_\odot} \\
1\ [\mathrm{L}] &= 8\ \mathrm{pc} \\
1\ [\mathrm{M}] &= 1.18 \cdot 10^8\ \mathrm{M_\odot} \\
1\ [\mathrm{V}] &= \sqrt{\frac{G \cdot 1\ [\mathrm{M}]}{1\ [\mathrm{L}]}} = 251.86\ \mathrm{km/s} \\
1\ [\mathrm{T}] &= \sqrt{\frac{1\ [\mathrm{L}]^3}{G \cdot 1\ [\mathrm{M}]}} = 0.031\ \mathrm{Myr}
\end{aligned}
$$

Table 5.1: Conversion table between the N-body units used in our work, and physical units. Here [L], [M], [T], and [V] are respectively the length, mass, time, and velocity units. The N-body units are such that $G = 1$, $M_{tot} = 1$, and $E_{tot} = -0.25$.

that we generate are truncated at $R = 1.7 = 13.6\,\mathrm{pc}$, with a total mass within this radius $M_{tot} = 1$. The particles have equal mass m. Particles are assigned Maxwellian velocities, then the system is virialised to dynamical equilibrium. Then, before inserting the black hole (BH) particle, we let the system evolve for a few crossing times. The system reaches a stable configuration, whose mass profile is no more perfectly reproduced by Eq. 5.4. The best fit for A and α on the mass profile of the stable configuration gives:

$$
\begin{aligned}
A &= 0.53\,, \\
\alpha &= 0.9\,.
\end{aligned}
\tag{5.8}
$$

In fact, the mass profile having these coefficients diverges from the original one as the distance R increases. On the other hand, in the region $R < 2$, where we study the BH infall, the discrepancy between the two mass profiles is small. The relaxed profile values are within 10% of the initial profile values. Nevertheless, for consistency we will use the values in eq. (5.8) for A and α hereafter. This results in values of $\ln\Lambda \simeq 10\%$ smaller than the ones given by a mass profile with coefficients $\alpha = 1.2$ and $A = 0.44$.

The BH particle is placed at the half-mass radius $R_{hm} \simeq 0.87$ with a circular orbit velocity, and its mass is $M_{BH} = 0.000\,528$. The background particles number varies from 16 000 to 2 million. The low particle number simulations are performed with the PP code, the intermediate and high number simulations with the treecode and the PM code. Fig. 5.3 shows the range of N for each code. This allows us to span a large range in particle number, so that the influence of granularity in the BH motion towards the Galaxy centre can be studied.

In contrast to the other models, we choose physical units for the PM code simulations. The conversion factors from physical units to N-body units are shown in table 5.1, where

n	outer	middle	inner
32	10.00	0.69	0.17
64	4.67	0.32	0.08
128	2.26	0.15	0.04

Table 5.2: Resolutions (i.e. cell sizes) of the different grid levels for the different choices of n in the PM code. n denotes the number of cells per dimension. The cell sizes of the different grid-levels (outer, middle and inner) are given in pc.

[L] denotes the unit length in N-body units, [M] the unit mass, [V] the unit velocity and [T] the unit time.

The parameters of the PM calculations are chosen in the following way: the grid sizes are kept constant at

$$\begin{aligned} R_{\text{system}} &= 140.0 \text{ pc} \\ R_{\text{out}} &= 9.6 \text{ pc} \\ R_{\text{core}} &= 2.4 \text{ pc} \end{aligned} \tag{5.9}$$

and are focussed on the center of mass of the "bulge" model, as sketched in fig. 5.2. To change the resolution we alter the number of grid cells per dimension from 32 up to 128. With this choice the cell sizes listed in table 5.2 are achieved.

To speed up the simulations, the time step in the PM code simulations should be as large as possible, but small enough to prevent spurious results. Therefore we started with a time step of 1 000 yr and reduced it to 200 and 50 yr. The results of the 200 yr and 50 yr time step do not differ from each other, therefore the global time step is chosen to be 200 yr. Conversely, the time step in the treecode and direct code simulations is variable and different for each particle. Time step values are in this case in the range 2–30 000 yr, with about 90% of them in the range 100–300 yr.

5.3 Results

We will now study the dependence of our results on the number of particles N in section 5.3.2, and compare the various N-body methods with identical initial realisations in section 5.3.3. After having convinced ourselves that the various techniques produce consistent results, we continue by studying the effect of softening/cell size (section 5.3.4) and black hole mass (section 5.3.6) on the value of the Coulomb logarithm in the inner part of the Galaxy.

Our simulations aimed at several goals. 1) understanding the scaling of the system dynamics with respect to the number of particles N, and within this scaling, how results from different methods compare with each other. 2) How, at a fixed value of N, the softening parameter influences the dynamics, changing the value of $\ln \Lambda$. The particle-mesh method does not make use of softening. The cell size in the PM code can be seen in this context as a

N	ϵ/ϵ_0	M_{BH}/m	ϵ/b_{min}	$\ln\Lambda$
16K	0	8.5	0	3.8
16K	1	8.5	2.6	3.6
80K	0	42.3	0	6.6
80K	0.01	42.3	0.03	6.0
80K	0.1	42.3	0.3	5.3
80K	1	42.3	2.6	4.8
80K	2	42.3	5.3	3.5
80K	8	42.3	21.2	2.8
80K	16	42.3	42.4	1.8

Table 5.3: Overview of the PP runs. N is the number of particles, ϵ is the softening parameter, $\epsilon_0 = 0.003\,735$, M_{BH}/m is the ratio between the BH mass and a particle mass, and ϵ/b_{min} the ratio between the softening parameter and the minimal impact parameter.

N	ϵ/ϵ_0	M_{BH}/m	ϵ/b_{min}	$\ln\Lambda$
80K	1	42.3	2.6	4.7
400K	1	211.3	2.6	5.0
2M	1	1056.5	2.6	4.9
80K	0.1	42.3	0.3	5.7
80K	2	42.3	5.3	4.1
80K	8	42.3	21.2	3.0
80K	16	42.3	42.4	2.0
80K	32	42.3	84.7	1.6
80K	1	84.5	1.3	5.4
80K	1	169.0	0.7	4.6
400K	1	422.6	1.3	4.6
400K	1	845.2	0.7	4.2

Table 5.4: Overview of the treecode runs. Meaning of symbols is the same as in table 5.3 above.

softening length. In our framework, it is crucial to understand the relation between the PP code and treecode softening parameter and the PM code cell size. 3) We also study how the BH mass influences the infall time. We doubled and quadrupled the BH mass, and observed how this affects the value of $\ln\Lambda$.

A resume of all the runs that we performed is reported in table 5.3 for the PP code runs, table 5.4 for the treecode runs, and finally table 5.5 for the PM code runs. In all of our runs, the system remains in equilibrium during the whole BH infall, with no significant mass loss from stellar escapes, and a mass profile independent of time.

N	n	m [$M_\odot$]	l [pc]	N_c [$\frac{\#}{\text{cell}}$]	m_c [$\frac{M_\odot}{\text{cell}}$]	$\frac{M_{BH}}{m_c}$	$\frac{l}{b_{min}}$	$\ln\Lambda$
80K	16	1475	1.60	46.3	68287.0	0.9	114.3	n/a
80K	32	1475	0.69	3.6	5375.4	11.6	49.3	1.9
400K		295	0.69	18.2	5375.4	11.6	49.3	2.1
2M		59	0.69	91.1	5375.4	11.6	49.3	2.2
80K	64	1475	0.32	0.4	546.3	114.5	22.9	3.0
400K		295	0.32	1.9	546.3	114.5	22.9	3.4
2M		59	0.32	9.3	546.3	114.5	22.9	3.0
80K	128	1475	0.15	0.04	61.9	1011	10.7	2.8
400K		295	0.15	0.2	61.9	1011	10.7	3.7
2M		59	0.15	1.0	61.9	1011	10.7	3.8
2M	256	59	0.076	0.1	7.4	8483	5.4	4.1

Table 5.5: Overview of the PM runs. N is the number of particles, n the number of grid cells per dimension, m the particle mass, l the intermediate grid cell size, N_c the average number of particles per cell, m_c the average mass of a cell, M_{BH}/m_c the ratio between the BH mass and the cell mass, and finally l/b_{min} the ratio between the cell size and the minimal impact parameter.

Before we start with the analysis of the results of our simulations, we report on the performance of the PP code and the treecode runs.

5.3.1 Code performance

In table 5.6 we give the average time, in seconds, needed to evolve the system for one N-body time unit (N-body time units are given in table 5.1). We report the data concerning the runs with $N = 80\,000$ and $M_{BH} = 0.000\,528$, for both the PP and the treecode runs. The PP runs have been executed on a partition of the GRAPE-6 (see section 1.3.2) including four GRAPE boards, for a peak-performance of about four TFlop/s. The treecode runs have been executed on the DAS-2 (mentioned in section 2.2.1), using a varying number of nodes, as reported in table 5.6. This varying number of PEs obviously affects the performance figures of the treecode runs; in order to obtain an homogeneous set of data, we normalised the figures to 32 PEs assuming a linear scaling, i.e. we halved the timing values measured on 16 PEs, and doubled the values measured on 64 PEs. The peak performance of the normalised system is 32 GFlop/s.

The normalised data are plotted in fig. 5.4, together with the PP code values (note the shift in the X-axis, in order to show the value for $\epsilon = 0$ on a log-log plot). We can see from the figure that the normalised treecode data are not heavily influenced by ϵ, while the PP code runs are much faster as ϵ increases. A possible explanation for this is that, as ϵ gets bigger, the chance for a close encounter gets smaller. Since the role of ϵ is to reduce the strength of the gravitational interaction at low interparticle distance to prevent close

PP code		treecode		
ϵ/ϵ_0	s/[T]	ϵ/ϵ_0	s/[T]	PEs
0	1400 ± 400	0.1	183 ± 11	32
0.1	1300 ± 200	1	529 ± 84	16
1	1038 ± 19	2	126.3 ± 5.2	64
2	785 ± 15	8	349 ± 38	16
8	485.3 ± 7.9	16	213.8 ± 4.3	32
16	440.5 ± 4.8	32	223 ± 12	32

Table 5.6: Performance of the PP and the treecode runs. We report the averaged number of seconds needed to advance the system for one N-body unit. For all runs we have $N = 80\,000$ and $M_{BH} = 0.000\,528$. The reference value for the accuracy parameter is $\epsilon_0 = 0.003\,735$.

encounters, a larger ϵ implies a lower chance for close encounters to occur. The time advance of the PP code is heavily affected by close encounters, as its high numerical precision can only be assured by a detailed, and costly, treatment of particle trajectories during close encounters. Hence, a reduced frequency of close encounters speeds up the execution of the PP code. The treecode does not include a special treatment for close encounters, hence its execution speed is not affected by a change in the close encounters frequency.

Fig. 5.4 also shows that the runs with the treecode are faster than those with the PP code, especially for low ϵ values. This effect is even much larger if we take into account that the PP runs have been performed on a four TFlop/s system, while the normalised treecode runs have been performed on a 32 GFlop/s system. Normalising the PP code runs on this performance would result in values 125 times slower. This is again the price of the high numerical precision of the PP code. In return for this, the energy conservation of the PP code is in the order of 10^{-6}, while the treecode conserves the energy within about 1%.

5.3.2 Dependence of $\ln \Lambda$ on N

In order to obtain a precise measure of $\ln \Lambda$, ideally one would run a direct N-body simulation with N of the order of the number of stars in the Galactic bulge, which amounts to $\sim 10^8$. Such high number makes a direct simulation unfeasible, and imposes the use of approximate methods instead. In order to evaluate the reliability of the approximate methods, we compared the PP code runs with the treecode runs. The PP code runs give a reliable picture of the system dynamics at low particle numbers, i.e. at high granularity. Using the treecode we can reach a much higher number of particles, up to two million, which still is two orders of magnitude lower than the real system. A comparison of the results from the two methods allows us to estimate the validity of the treecode runs, up to 2 million particles. Then we can compare the treecode runs and the PM runs, in order to validate the results from the latter, which has the capability to simulate systems of about 100 million stars. In this way we will eventually be able to study the infall of a BH into the Galactic centre in a simulation

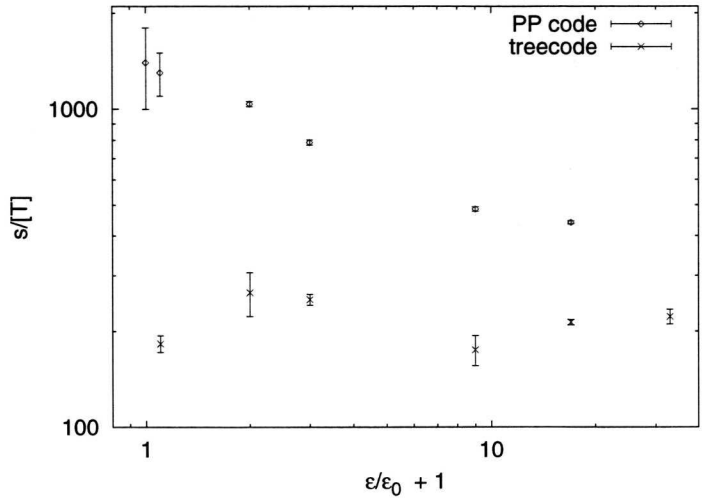

Figure 5.4: Performance of the PP and the treecode runs. We plot here the averaged number of seconds needed to advance the system for one N-body unit. For all runs we have $N = 80\,000$ and $M_{BH} = 0.000\,528$. The PP code runs are executed on a GRAPE-6 partition including four GRAPE boards, the treecode runs are executed on the DAS-2, with varying number of nodes. The values plotted here are normalised to 32 PEs. Note the shift in the X-axis, where we plot $\epsilon/\epsilon_0 + 1$.

environment with a realistic value of N.

In fig. 5.5 we show the evolution of the BH distance from the centre of mass of the system for three treecode simulations. N varies from 80 000 to 400 000 and 2 million, with $\epsilon = \epsilon_0 = 0.003\,735$, corresponding to about 0.03 pc. In fig. 5.6 we present a similar figure from PM code simulations. Here is $N \in \{80\,000, 400\,000, 2\,000\,000\}$, with 32 cells per dimension, resulting in a cell size of about 0.69 pc.

Fig. 5.5 and 5.6 show that increasing N results in a much smoother motion of the BH in its infall towards the centre of the Galaxy. The BH infall rate (though very different in the two cases) is not much affected by a change in N. Accordingly, the value of $\ln\Lambda$ for each of the two sets above is consistent, as values in table 5.4 (first three rows) and table 5.5 (rows with $l = 0.69$) show.

In order to study further the extent of the influence of N on the infall rate of the BH, and hence in $\ln\Lambda$, we compare in fig. 5.7 results from PM code simulations with increasing grid refinement, and extreme difference in N. To quantify the grid resolution, we use the cell length at intermediate refinement, which is the cell length pertaining to the physical region where the BH evolves for most of its infall. We measure this length in units of $\epsilon_0 = 0.003\,735$, which makes the comparison with the softening parameter of the treecode easier. N has no strong influence on the infall rate, except for the case where the cell size is $l = 0.15$ pc $\simeq 5\epsilon_0$. In this case the simulation with $N = 80\,000$ (data not reported in the figure), shows an incorrect BH infall, comparable to the case $l = 0.32 \simeq 10\epsilon_0$. This can be explained by the

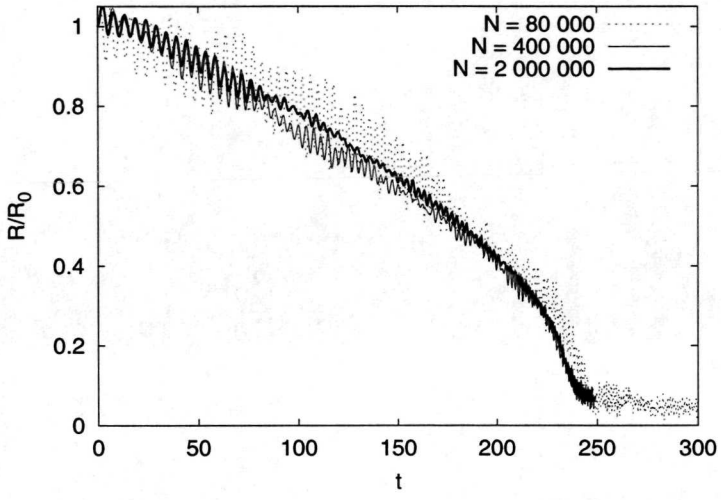

Figure 5.5: Time evolution of the radial distance of the black hole to the Galactic centre. The various curves (identified in the top right corner) present results obtained with the treecode. the X-axis is presented in N-body time units: one N-body time unit corresponds to about 0.031 Myr. The distance of the black hole to the Galactic centre (Y-axis) is given in terms of its initial distance. In these simulations is $\epsilon = 0.003\,735 \simeq 0.03$ pc and $M_{BH} = 0.000\,528$.

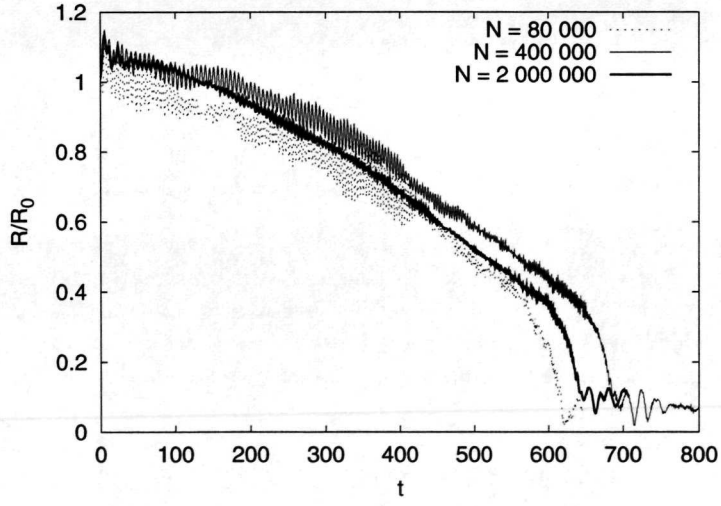

Figure 5.6: Same as fig. 5.5 above, but for PM code simulations. The intermediate grid cell size is here $l = 0.69$ pc, and $M_{BH} = 0.000\,528$.

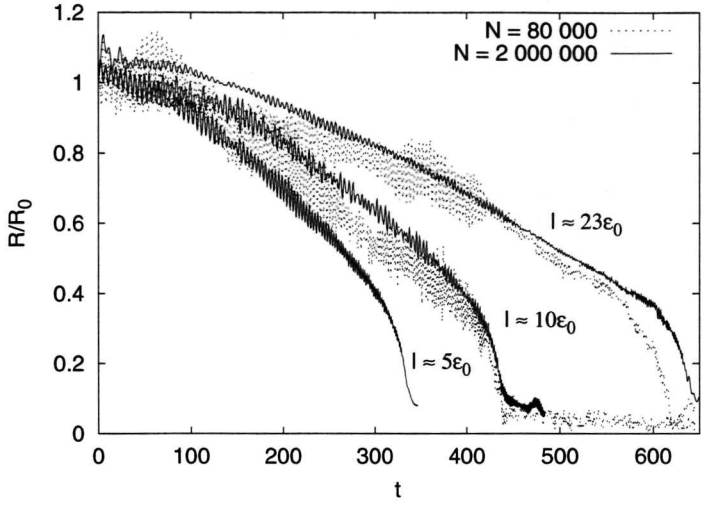

Figure 5.7: Black hole infall at various cell sizes, and large difference in N. Results here are from PM code simulations. The case $N = 80\,000$, $l \simeq 5\epsilon_0$ is not shown for readability reasons, since it would overlap with the $l \simeq 10\epsilon_0$ results.

fact that in the low l, low N case, the cells are so small, and the particles so few, that many cells in the PM grid are empty (see also the N_c column in table 5.5, which gives the average number of particles per cell). When $N_c \ll 1$, the density field is incorrect, with many grid points having a null value, because the corresponding cell is empty. In this condition, the gravity field computed by the PM code becomes unreliable, affecting the numerical results, as in the simulation with $N = 80\,000$ and $l \simeq 5\epsilon_0$.

5.3.3 Comparison of the codes

In this section we compare the results obtained from the various codes, to check their consistency. The comparison of the PM results with the two other codes results is particularly critical, since the PM code computes forces using a different mathematical approach, i.e. a grid based force derivation vs a direct particle-particle computation for the PP code, or particle-multipole computation for the treecode. A consequence of this is a different parameter to tune the accuracy of the simulation, namely the cell size l for the PM code, and the softening length ϵ for the other two codes. We will study here how these two parameters influence the black hole infall.

In fig. 5.8 we show the time evolution of the galactocentric BH distance R simulated by the PP code, accompanied by a plot of the time evolution of $\Delta R/R_{PP}$ for treecode and PM simulations, where $\Delta R = (R - R_{PP})$. The relative difference $\Delta R/R_{PP}$ remains small for a large fraction of the infall, and the final discrepancy is mostly due to the small values of the quantities at that point, which are likely to amplify relative differences. As the following

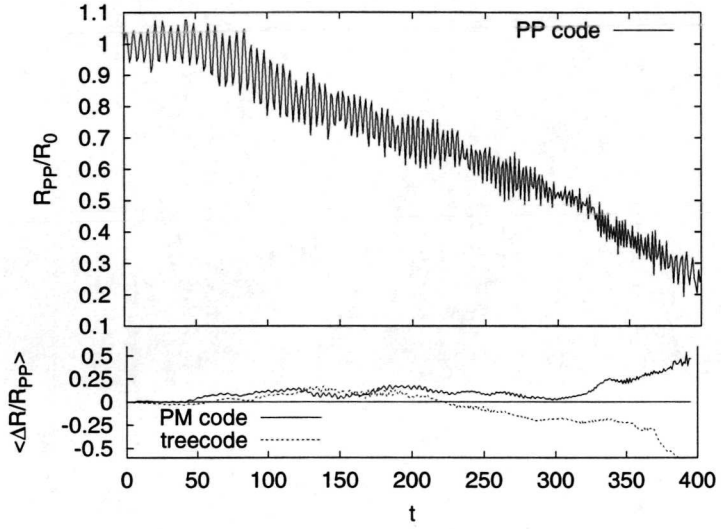

Figure 5.8: Top panel shows a black hole infall simulated by the PP code, with $N = 80\,000$, $M_{BH} = 0.000\,528$ and $\epsilon = 8\epsilon_0$. Bottom panel shows a comparison of the PP results with treecode and PM results. Parameter values are in all cases the same, except for the PM cell size, which is $l = 10\epsilon_0$. Plotted values are averages over 10 time units.

figures also show, the BH infall is predicted with very good consistency between the codes.

In fig. 5.9 selected treecode runs with $N = 80\,000$ and increasing ϵ are compared with the direct code runs having the same values of N and ϵ. At the same time, the figure shows how the infall time increases (and implicitly how $\ln\Lambda$ decreases), as ϵ increases. Fig. 5.9 and table 5.7 show that the results from the treecode, the PP code, and the PM code are in good agreement. The agreement of the results from the three methods, and the scaling of $\ln\Lambda$ with ϵ, will be further studied quantitatively in section 5.3.5.

In order to understand how the cell length l of the PM code and the softening parameter ϵ of the PP code and treecode relate with each other, we compare in fig. 5.10 the results from the PM code and treecode simulations with 80 000 particles. The BH infall as shown in fig. 5.10 depends on the value of l or ϵ. Remarkably, l and ϵ seem to play the same role not only qualitatively, but also quantitatively: in a PM run, a given value of l induces an infall which is very similar to the infall, in a treecode run, with ϵ assuming that same value. In section 5.3.5 this relation will be studied further.

5.3.4 The effect of softening/grid

The influence of the softening parameter on the BH dynamics has been studied by running a number of simulations with the three codes. In table 5.7 we report the value of $\ln\Lambda$ obtained from our simulations. For the PP code and treecode simulations, we increase ϵ from 0 to $32\epsilon_0 = 0.1195 \simeq 0.96\,\mathrm{pc}$. For the PM code, we increase l from $2.5\,\epsilon_0$ to $23\,\epsilon_0$. In all cases is

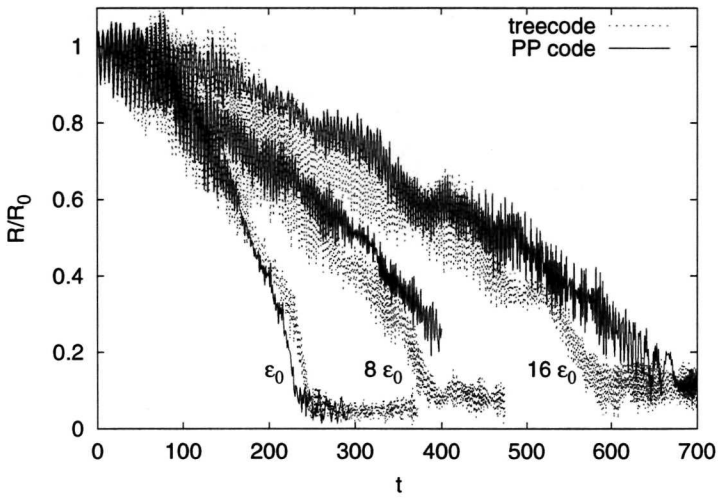

Figure 5.9: Comparison of results from the PP code with results from the treecode, at different values of ϵ. For all cases shown here is $N = 80\,000$ and $M_{BH} = 0.000\,528$. The PP simulation with $\epsilon = 8\epsilon_0$ has been already shown in fig. 5.8.

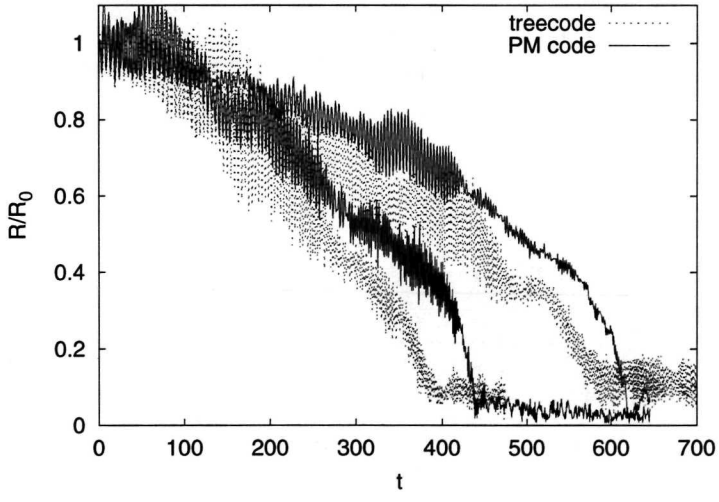

Figure 5.10: Comparison of PM results with treecode results. PM simulations have cell size l equal to resp. $10\epsilon_0$ and $23\epsilon_0$; softening parameters in the treecode runs are resp. $8\epsilon_0$ and $16\epsilon_0$. In all the above cases, is $N = 80\,000$ and $M_{BH} = 0.000\,528$.

ϵ/ϵ_0	PP code	treecode	l/ϵ_0	PM code
0	6.6			
0.01	6.0			
0.1	5.3	5.7		
1	4.8	4.7		
2	3.5	4.1	2.5	4.1
8	2.8	3.0	5	3.8
16	1.8	2.0	10	3.0
32		1.6	23	2.2

Table 5.7: $\ln\Lambda$ versus ϵ from PP code, treecode, and PM code runs. For the PP code and treecode runs is $N = 80\,000$. For the PM code runs is $N = 2$ million. The reference value for the accuracy parameter is $\epsilon_0 = 0.003\,735$.

$M_{BH} = 0.528 \cdot 10^{-3} \simeq 62\,300\,\mathrm{M}_\odot$.

For the PP code and the treecode, we selected $N = 80\,000$ as a suitable value. The relaxation time eq. (1.2) is for this value of $N\,t_r \simeq 0.1N/\ln N \cdot R^{3/2} \simeq 2000$, about one order of magnitude larger than the typical BH infall time, so that the system is collisionless, and we can confidently use the treecode to simulate it. With this choice for N, the BH mass is $M_{BH}/m \simeq 42.3$, (see table 5.4). As a cross-check, we ran two PP runs with $N = 16\,000$ which, as expected, gave incorrect results (see table 5.3). This is due to both a too small M_{BH}/m ratio, and a too short relaxation time ($t_r \simeq 400$ in this case). We did not increase ϵ above $32\,\epsilon_0$, since at this point ϵ is already much bigger than b_{min} (see table 5.4), and the infall time is now close to t_r.

For the PM code simulations, we used $N = 2$ million in order to have enough particles to fill all the cells, even for the simulations with a small l. As table 5.5 shows, for $l = 0.076\,\mathrm{pc} \simeq 2.5\,\epsilon_0$ the average number of particles per cell is already $N_c = 0.1$. Since a PM simulation gives incorrect results for $N_c \ll 1$ (see also the discussion at the end of section 5.3.2), we did not decrease l below $2.5\,\epsilon_0$.

The decrease of the value of $\ln\Lambda$ as ϵ or l increases is clear from table 5.7. In the next section we focus on the relation between Λ and ϵ, and provide a fitting formula for $\ln\Lambda(\epsilon)$. We use hereafter ϵ to refer either to the softening length of the PP and treecode, or the cell size of the PM code. As shown on fig. 5.10 and discussed above, these two parameters play the same role even quantitatively in affecting $\ln\Lambda$. In this respect, we refer to ϵ as a generic accuracy parameter.

5.3.5 Determination of $\ln\Lambda$

We will study here the relation between ϵ and $\ln\Lambda$. As just said above, in this context ϵ will be used as the accuracy parameter, and it will refer to either the softening length used in the PP and treecode, or to the cell size in the PM code.

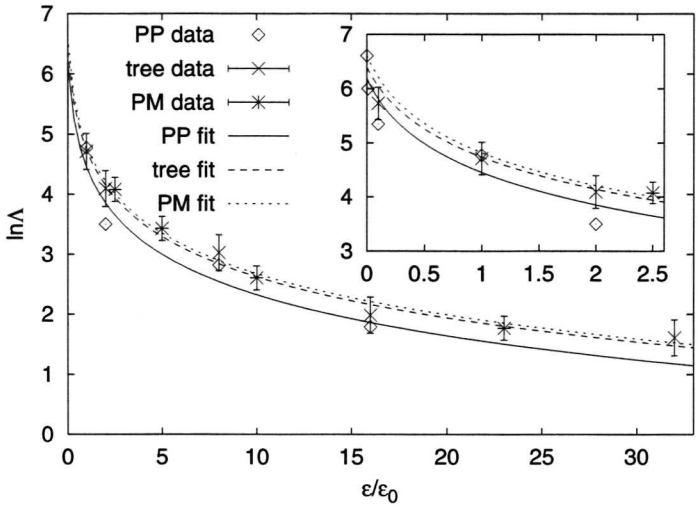

Figure 5.11: $\ln\Lambda$ vs ϵ, and best fit for $\ln\Lambda = K - \ln(a+\epsilon)$. Values for K and a are given in table 5.8. The inset in the figure is a magnification of the low ϵ region. In all cases is $M_{BH} = 0.000\,528$. For the PP and treecode runs is $N = 80\,000$, for the PM code runs is $N = 2\,000\,000$. Error bars are omitted from the PP values to improve readability. For the same reason, $\ln\Lambda$ values for $\epsilon/\epsilon_0 < 1$ are shown only in the inset.

A mathematical expression for the relation between ϵ and $\ln\Lambda$ can be found by considering how softening affects two body scattering. The role of ϵ is to prevent too close stellar encounters. In this respect, the effect of introducing a softening length is to increase the minimal impact parameter. Hence, we can define an effective impact parameter $b_{eff} = b_{min} + \epsilon$, and we modify eq. (5.3) to become:

$$\ln\Lambda = \ln\frac{b_{max}}{b_{eff}} = \ln\frac{b_{max}}{b_{min}+\epsilon}\,. \tag{5.10}$$

We will now fit this equation with the values reported in table 5.7. In order to perform the fit, we change eq. (5.10) in a more suitable form, as follows:

$$\ln\Lambda = \ln b_{max} - \ln(b_{min}+\epsilon) = K - \ln(a+\epsilon)\,. \tag{5.11}$$

We will refer to b_{max} and b_{min} as the theoretical values of the maximal and minimal impact parameters, as they can be obtained from eq.s (5.2) and (5.3), and K and a as the corresponding experimental values obtained with the fit.

The best fits for K and a with respect to simulation values are reported in table 5.8 for all codes. Such fits have been performed with a fixed value for R_0, i.e. the $R_0 = R_{hm}$. In fact, the not perfectly circular orbit of the BH results in an oscillatory behaviour for the BH

	PP code	treecode	PM code
K	-0.94 $\pm$ 0.21	-0.64 $\pm$ 0.10	-0.59 $\pm$ 0.05
$a \cdot 10^{-3}$	0.80 $\pm$ 0.28	0.88 $\pm$ 0.20	0.74 $\pm$ 0.08
$\Delta(\ln \Lambda)$	0.6	0.3	0.2

Table 5.8: Best values for the parameters K and a, and error on $\ln \Lambda$ for the fit of $\ln \Lambda = K - \ln(a + \epsilon)$.

galactocentric radius. In this case, having R_0 fixed could not be an appropriate choice for the fit. We checked whether having R_0 as a free parameter in the fit leads to different results in $\ln \Lambda$. We obtained values for $\ln \Lambda$ within the error bars in fig. 5.11, and values for R_0 within $R_{hm} \pm 0.05$. We can conclude that, although the galactocentric BH radius does not decrease smoothly, but in an oscillatory fashion, having R_0 fixed to the actual initial BH radius in the simulations leads to correct fits for the value of $\ln \Lambda$. With respect to the PM values, a further peculiarity is that when the BH enters the finest grid area, i.e. approximately at $R = 0.3$, the value of l decreases (see section 5.2.3 and fig. 5.2). This causes b_{eff} to become smaller, increasing the value of $\ln \Lambda$. In fact, a fit of the PM data limited to values of $R > 0.3$ gives values of $\ln \Lambda$ systematically higher by $\simeq 0.3 \simeq 2\Delta(\ln \Lambda)$.

From the PP code value of K in table 5.8 we obtain for b_{max} the experimental value $b^E_{max} = e^K \simeq 0.39$. This value is much smaller than what one would expect. Since b_{max} has the meaning of the maximal impact parameter, a natural choice is to assign it a value of the order of the system size, which in our case would result in $b_{max} = 2$. The maximal radius for dynamical friction in our system is then about one quarter of what it is customarily assumed. PM and treecode values are slightly higher, but still much smaller than $b_{max} = 2$. Also a is smaller than the theoretical value $b_{min} = G \cdot (M_{BH} + m)/v^2_{typ} = 1.41 \cdot 10^{-3}$, by a factor 3. The a value for all codes is perfectly consistent.

An explanation for the discrepancy between the values of b_{max} and b^E_{max} is that the BH, while moving to the Galactic centre, is off-centre with respect to the density peak (in fact the BH is spiralising towards it). With respect to the BH position, the density distribution is then asymmetric. This density peak clearly has a greater influence on the BH dynamics, contributing more than the other regions of the system to the dynamical friction on the BH. This leads to a value of b_{max} affected by the galactocentric BH radius. This approach is studied in detail by Hashimoto *et al.* (2003), who propose the galactocentric radius as a value for b_{max} in the context of the spiral-in of satellite galaxies.

In our simulations, the galactocentric radius varies from $R \simeq 0.9$ at the beginning of a simulation, to $R \simeq 0$ at the end of it. The value of b^E_{max} that we find is within this range, and it can be interpreted as an order 0 estimate of a maximal impact parameter that depends on the galactocentric BH radius.

In order to explore this aspect further, we simulated the infall of the same BH, starting at the quarter mass radius $R_{qm} \simeq 0.43$, for ϵ ranging from 0 to $16\epsilon_0$. What we expect is a smaller value of b^E_{max}, hence smaller values of $\ln \Lambda$. All simulations are performed with the treecode, except for the $\epsilon = 0$ case, which is simulated with the PP code. Our results are

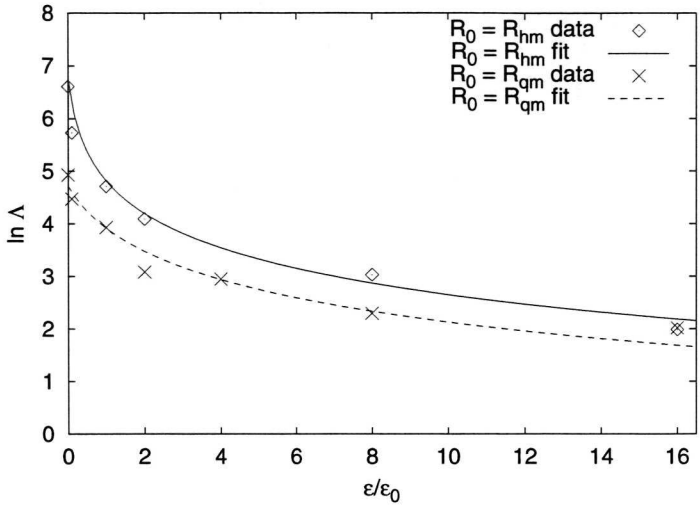

Figure 5.12: Comparison of $\ln\Lambda$ vs ϵ at different initial galactocentric BH radii. The smaller values of $\ln\Lambda$ for the cases with $R_0 = R_{qm}$ indicate that b_{max} is influenced by the galactocentric BH radius.

in fig. 5.12. We can see there that the values of $\ln\Lambda$ are smaller for the cases when the BH starts at the quarter mass radius. A fit on these data gives $K \simeq -1.1$, which implies $b^E_{max} \simeq 0.33$, which is smaller than the value of b^E_{max} obtained for the BH starting from the half mass radius. Our findings support the argument of Hashimoto *et al.* (2003).

5.3.6 Varying black hole mass

We also studied the effect of a variable BH mass on the value of $\ln\Lambda$. We simulated, using the treecode, the infall of a BH of mass two times and four times larger than the default mass $M_0 = 0.000\,528 \simeq 0.62 \cdot 10^5 \mathrm{M}_\odot$. We studied this infall in both the 80 000 particles configuration, and the 400 000 particles configuration. In all cases, we used our standard value for ϵ, i.e. $\epsilon_0 = 0.003\,735$. In fig. 5.13 the distance r of the BH from the centre of mass of the system is shown for all the cases mentioned above, together with the $M_{BH} = M_0$ cases. From eq. (5.11) and table 5.8, the appropriate value for $\ln\Lambda$ in the above cases is:

$$\begin{aligned} \ln\Lambda &= K - \ln(a + \epsilon_0) \pm \Delta = \\ &\quad -0.64 - \ln(0.000\,88 + 0.003\,735) \pm 0.3 \simeq 4.7 \pm 0.3 \,. \end{aligned}$$

We also show in fig. 5.13 the analytic curve $r(t)$, as given by eq. (5.5), with $\ln\Lambda = 4.7$. An error bar gives, for each analytical curve, the spread corresponding to a variance $\Delta(\ln\Lambda) = 0.3$.

The results shown in fig. 5.13 are consistent with the hypothesis that a variation in the BH mass has a little effect in the value of $\ln\Lambda$. In fact, $\ln\Lambda$ shows a logarithmic dependence on M_{BH} through the parameter b_{min}, which depends linearly on M_{BH} (see eq.s (5.2)

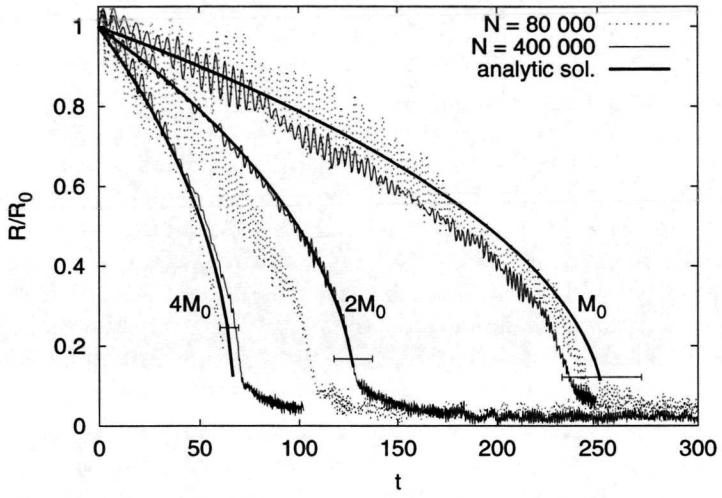

Figure 5.13: Black hole infall for different values of the BH mass, and different values of N. Simulations are performed with the treecode. Simulation results are compared with the analytic solution, eq. (5.5), with $\ln\Lambda$ obtained from eq. (5.11) and table 5.8. The error bars at the bottom of the analytic curves correspond to a variance $\Delta(\ln\Lambda) = \pm 0.3$.

and (5.3)). Assuming that also the experimental value a depends linearly on M_{BH}, we obtain $\ln\Lambda \simeq 4.6 \pm 0.3$, and $\ln\Lambda \simeq 4.4 \pm 0.3$ respectively for the 2 M_{BH} case and the 4 M_{BH} case. This results in a small displacement towards the right of the corresponding analytic curves in fig. 5.13, which does not affect the conclusions that can be drawn from the figure. The theoretical curve fits very well with the $M = 2\,M_0$, $N = 400\,000$ case. The other simulation curves are within, or very close to, the error in $r(t)$ associated to the error in $\ln\Lambda$. We can conclude that a variation in the mass of the infalling object has little influence in the value of $\ln\Lambda$, which is important in view of extending this work to the case of the infall of a star cluster.

The fitting formula for $\ln\Lambda$ vs ϵ was obtained from simulations with $M_{BH} = M_0$. This formula predicts $\ln\Lambda$ for the cases with $M_{BH} > M_0$ with a very good accuracy, showing that it can be applied in a more general context, in order to forecast the value of the Coulomb logarithm.

Fig. 5.13 also shows a damping in the BH infall at very small values of R, especially for the $N = 400\,000$ case. This effect, described in section 5.2.5, is clearer in the $N = 400\,000$ case, since the particle density is higher in this case, compared to the $N = 80\,000$ case.

5.3.7 Comparison with related work

Milosavljević & Merritt (2001) study the dynamical evolution of two black holes, each one

at the centre of a power law cusped galaxy core. They simulate the merging of the two galaxies, and observe the evolution of the two black holes, which form a hard binary at the centre of the merged galaxy. In section 3 of their paper they discuss the value of $\ln\Lambda$ in their simulations. They measure the decay rate of the two black holes, and compare this value with theoretical estimates. When they compare their experimental decay rate with an estimate for the case of the infall of an isolated black hole, they find a theoretical estimate about 6 times lower than the measured value, under the assumption that $\ln\Lambda \simeq 1.6$. If the value of $\ln\Lambda$ is not theoretically pre-determined, and is instead obtained from the decay rate equation, the result is $\ln\Lambda \simeq 10$. Similarly, they compare the experimental value with an estimate for the case of two mutually spiralling spherical distributions of matter. In this case they assume $\ln\Lambda \simeq 1.0$, and obtain an estimate for the decay rate about a factor of 2 lower than the observed value. Determining $\ln\Lambda$ from the measurement would give in this case $\ln\Lambda \simeq 1.87$. The values of $\ln\Lambda$ that we find are between the two values above.

The value for $\ln\Lambda \simeq 1$ that they assume in their theoretical estimates, comes from a derivation that they present in appendix A of the same work. This derivation is based on results of Maoz (1993). Under the assumption that the stellar density obeys a power law centered on the BH position:

$$\rho(r) = \rho_0 \left(\frac{r}{b_{min}}\right)^{-\alpha} , \tag{5.12}$$

they obtain $\Lambda \simeq 1/\alpha \simeq 1$, which actually implies $b_{max} \simeq b_{min}$, whereas it is customary to consider $b_{max} \gg b_{min}$.

Their assumption in fact is valid only when the BH is close to the centre of the power law distribution. In their context this is true when: 1) the separation between the two BHs is much larger than the half mass radius of the two galaxies. In this case each BH is at the centre of its own galaxy, and at the same time its motion is not yet heavily perturbed by the other galaxy. 2) the BH binary has hardened, and occupies the centre of the merged galaxy.

During the transient phase, when the two BHs have not yet formed a binary, the density distribution that affects the motion of the BHs is double-cusped, with a BH in each of the two cusps. This is substantially different from the density distribution modelled by eq. (5.12).

This qualitative argument would make the density distribution in eq. (5.12) inapplicable during the transient phase, and could explain why Milosavljević & Merritt (2001) find a higher than expected value of $\ln\Lambda$ in the transient. The analytical evaluation of $\ln\Lambda$ according to the technique used by them is by no means trivial, when symmetry arguments cannot be straightforwardly applied. We will address this issue in future developments of the present work; the theory of linear response of Colpi & Pallavicini (1998) could be very useful in this context.

5.4 Applications to star clusters

Recent observations of the Galactic Centre have revealed a population of very young clusters with ages less than 10 Myr. The presence of such stars inside the inner parsec of the Galaxy

is puzzling, as the strong tidal field in the Galactic centre easily prevents star formation. The origin of these stars is therefore debated (Gerhard, 2001; McMillan & Portegies Zwart, 2003). Morris (1993) proposed that a star cluster at some distance from the Galactic centre could spiral-in due to dynamical friction (see also Gerhard, 2001). The efficiency of dynamical friction depends sensitively on the actual value of the Coulomb logarithm $\ln\Lambda$.

5.4.1 Sinking of massive black holes in the Galactic centre

We performed N-body simulations for a large range of conditions. In section 5.3.2 we varied the number of particles, in section 5.3.4 we varied the size of the object, and in section 5.3.6 we varied its mass. With direct N-body simulations we measured the actual value of the Coulomb logarithm $\ln\Lambda$. We study the behaviour of $\ln\Lambda$ for various types of N-body solvers and particle numbers. We also study the behaviour of $\ln\Lambda$ as a function of the softening length ϵ. Only the direct N-body code can perform a true measurement of the Coulomb logarithm, because it is able to resolve even the smallest length scales and time scales. This, however, makes the direct code very slow and, even using the very fast GRAPE-6 special purpose device, we are able to perform simulations with only 10^5 particles. This is a small number compared to the actual number of stars in the Galactic centre. With approximate methods (treecode and particle-mesh) we are able to increase the number of particles up to 2 million. The cost of this is a lower accuracy in calculating stellar motion below a typical length scale ϵ. We studied how this length scale influences $\ln\Lambda$, by affecting the value of the minimal impact parameter.

5.4.2 Young dense clusters in the Galactic centre

The study of the dependence of $\ln\Lambda$ on ϵ described above is also of astronomical interest, because ϵ can be interpreted as the typical length of a finite size infalling object. Based on this, our analysis of the dependence of $\ln\Lambda$ on ϵ can be seen as a first approach to the study of the infall of a star cluster of typical size ϵ toward the Galactic centre. We found (see fig. 5.11) that the value of $\ln\Lambda$ decreases quite rapidly as ϵ increases, with the logarithm argument $\Lambda \propto 1/\epsilon$. The typical size of the compact young clusters observed in the Galactic bulge is $\simeq 0.3\,\mathrm{pc}$ (Figer *et al.*, 1999), which corresponds to $\epsilon \simeq 10\epsilon_0$. With this value of ϵ, from eq. (5.11) and table 5.8, we obtain $\ln\Lambda \simeq 2.9$, about 60% less than the value for a point mass. The infall time is roughly doubled. For our choice of object mass, $M \simeq 62\,300\ \mathrm{M}_\odot$, and initial galactocentric radius, $R_0 \simeq 7$ pc, we have an infall time that increases from $\simeq 6\,\mathrm{Myr}$ for the point mass, to $\simeq 12.5\,\mathrm{Myr}$ for an object of typical size $\simeq 10\epsilon_0 \simeq 0.3\,\mathrm{pc}$.

We also studied the uncertainty associated with the maximal impact parameter b_{max}. We found that for an infall to the Galactic centre, the infalling object is mostly influenced by the density peak at the Galactic centre itself. A good choice for b_{max} is then $b_{max} \simeq \beta R_0$, where R_0 is the initial galactocentric radius, and $\beta \simeq 0.5$

5.5 Discussion

We simulated the evolution of a massive particle in a sea of lighter particles in a self gravitating system. The main goal of this simulations is to obtain an accurate value of the Coulomb logarithm ($\ln\Lambda$). This helps us to understand the dynamics of the Galactic bulge and the rate at which intermediate mass black holes sink to the Galactic centre. We also study the effect of the finite size of the inspiraling object.

We ran both N-body particle-particle (PP) simulations, softened treecode simulations, and particle-mesh (PM) simulations. The comparative simulations are performed for 80 000 particles, and all result in the same value of $\ln\Lambda$. For a point particle near the Galactic centre we find $\ln\Lambda = 6.6 \pm 0.6$. In addition we measure the change in the Coulomb logarithm with respect to the softening parameter ϵ, which reveals $\Lambda \propto 1/\epsilon$. We argue that ϵ can be interpreted as the typical length of a finite size object, such as a star cluster, so that $\ln\Lambda$ as a function of ϵ can be seen as a first approximation of the dependence of the Coulomb logarithm on the size of an infalling star cluster.

We also observed a value of the maximal impact parameter b_{max} different from the customarily assumed value, which is proportional to the system size. We found that our results are more consistent to a value of b_{max} linearly dependent on the BH galactocentric radius, which is in agreement with Hashimoto *et al.* (2003).

We performed simulations with up to two million particles using a treecode. The obtained value of $\ln\Lambda$ does not depend on the number of particles. Apparently, 80 000 particles is already enough to eliminate any granularity for our choice of initial conditions. The results of the treecode, at the low N-limit, are in excellent agreement with the PP simulations, and we find the same scaling with respect to ϵ. Increasing the black hole mass reduces the time scale for spiral-in as expected from theory (see McMillan & Portegies Zwart, 2003).

Finally we compared the results of our PP and treecode simulations with a particle mesh (PM) method. We compared the methods for N up to two million. The results of our PP, treecode, and PM calculations are in good agreement. The cell size in the PM model is directly comparable to the softening length ϵ in the PP and tree methods.

This work is a first step in the direction of performing a simulative study of the infall of a young star cluster to the Galactic centre (see section 5.4.2). As discussed in section 1.7, a star-by-star simulation of a cluster infall is problematic. The total number of particles, including both the cluster particles and the Galactic centre particles, is by far larger than the number a direct code can manage. On the other hand, the use of a treecode would lead to an incorrect treatment of the cluster dynamics, resulting in a too fast, unrealistic cluster evaporation. A solution for this problem is the development of a hybrid code, consisting of a direct code "phase" that is responsible of the simulation of the cluster, and a treecode "phase" that simulates the galactic centre. The data exchange between the two phases is negligible: the treecode input is the current mass of the cluster, and the direct code input is the current value of the galactic gravitational force.

A hybrid architecture of the kind described in part I is an ideal hardware platform for

this hybrid code simulations, and the pseudo-particle treecode described in chapter 4 lends itself very well to being included in the hybrid code as its low accuracy component.